Geochemical Perspectives Letters

Mobility of chromium in high temperature crustal and upper mantle fluids

J. Huang[1*], J. Hao[1,2], F. Huang[1,3], D.A. Sverjensky[1]

OPEN ACCESS

doi: 10.7185/geochemlet.1926

Abstract

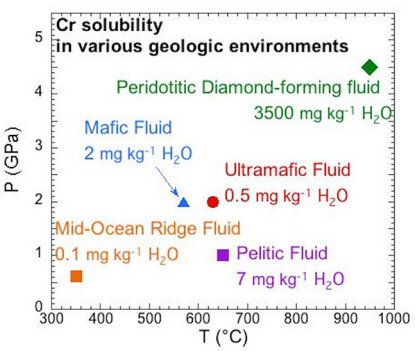

Chromium is mobile in ultramafic magmas but its mobility in high temperature fluids has long been unclear. Studies of some chromium-rich ophiolites have suggested chromium mobility in upper mantle fluids. However, the mechanism is poorly understood because Cr(III) is so insoluble in water. We used previous estimates of aqueous Cr species and published experimental and *ab initio* studies of the solubility of Cr_2O_3 in HCl and KCl fluids at 500–1200 °C and 0.1–6.0 GPa together with the Deep Earth Water Model to calibrate a thermodynamic equation of state for the Cr(II) complex $CrCl(OH)^0$. Our model predicted low Cr solubilities (0.1 mg kg^{-1} H_2O) in a mid-ocean ridge fluid and very high solubilities (3500 mg kg^{-1} H_2O) in saline, peridotitic diamond-forming fluid consistent with expectations for these environments. In pelitic, mafic eclogitic, and serpentinite fluids, predicted Cr solubilities varied widely depending on the oxygen fugacity and Cl concentration. The predicted predominance of Cr(II) in deep fluids and Cr(III) in minerals suggests that precipitation of Cr mineral components is a redox reaction.

Received 18 March 2019 | Accepted 26 July 2019 | Published 13 November 2019

Introduction

Chromium is a mobile element in ultramafic or mafic magmas but its mobility in high temperature fluids has long been unclear. Recent studies of chromium-rich geological settings have suggested that chromium could be mobile in deep crustal and upper mantle fluids. For example, fluid inclusions in chromite from New Caledonia (Johan *et al.*, 2017) and in diopsidites and anorthosites associated with chromite and uvarovite from Oman (Akizawa *et al.*, 2016) suggest the mobility of Cr in hydrothermal fluids at temperatures of about 500 to 800 °C. In addition, garnet inclusions in peridotitic diamonds are characteristically Cr-rich (Stachel and Harris, 2008), suggesting that Cr could be involved in the metasomatic processes of diamond formation under sub-solidus conditions. However, aqueous Cr^{3+} is highly insoluble in water at near neutral pH (Rai *et al.*, 1987; Saleh *et al.*, 1989; Ziemniak *et al.*, 1998; Sander and Koschinsky, 2000), so a mechanism for Cr mobility has remained mysterious.

One potential mechanism for Cr solubility at high temperatures is the likelihood of an aqueous Cr(II) oxidation state (Fig. 1a,b). Many metals exhibit the tendency for a lower oxidation state in aqueous solution at elevated temperatures, *e.g.*, aqueous Cu^+ *vs.* Cu^{2+} (Mei *et al.*, 2013), Fe^{2+} *vs.* Fe^{3+} (Testemale *et al.*, 2009), and Eu^{2+} *vs.* Eu^{3+} (Sverjensky, 1984). To investigate the potential mobility of Cr(II) and Cr(III) in deep fluids, we predicted the solubility of Cr oxide minerals by updating previous estimates of aqueous Cr species (Shock *et al.*, 1997; Hao, 2016) in the Deep Earth Water (DEW) model (Sverjensky *et al.*, 2014). We then regressed experimental solubility data for Cr_2O_3 to characterise a proposed new Cr(II) complex $CrCl(OH)^0$ and obtain a predictive model for Cr solubility. Our model was applied to a wide range of geological settings: mid-ocean ridges (MOR), subduction zones and the subcontinental lithospheric mantle environment of diamond formation. Models and calculation methods are given in the Supplementary Information (SI).

Results

Analysis of solubilities in solutions. We used published solubilities of Cr_2O_3 in HCl-rich fluids containing 1.646 mol kg^{-1} and 2.249 mol kg^{-1} HCl from 500–700 °C and 0.1–1.0 GPa (Watenphul *et al.*, 2014) to test the predicted properties of aqueous Cr species. The thermodynamic properties of eskolaite (Cr_2O_3) and picrochromite ($MgCr_2O_4$) were obtained from published experimental data (SI). The data points in Figure 1c,d represent the logarithms of measured Cr concentration *vs.* pressure. Cr concentrations at 400 °C were not considered in our analysis because the reactions may not have reached

1. Department of Earth and Planetary Sciences, Johns Hopkins University, Baltimore, MD 21218, USA
2. Laboratoire de Geologie de Lyon, Observatoire de Lyon, Universite Claude Bernard Lyon1, 69007 Lyon, France
3. Rensselaer Polytechnic Institute, NY 12180, USA
* Corresponding author (email: jyhuang@jhu.edu)

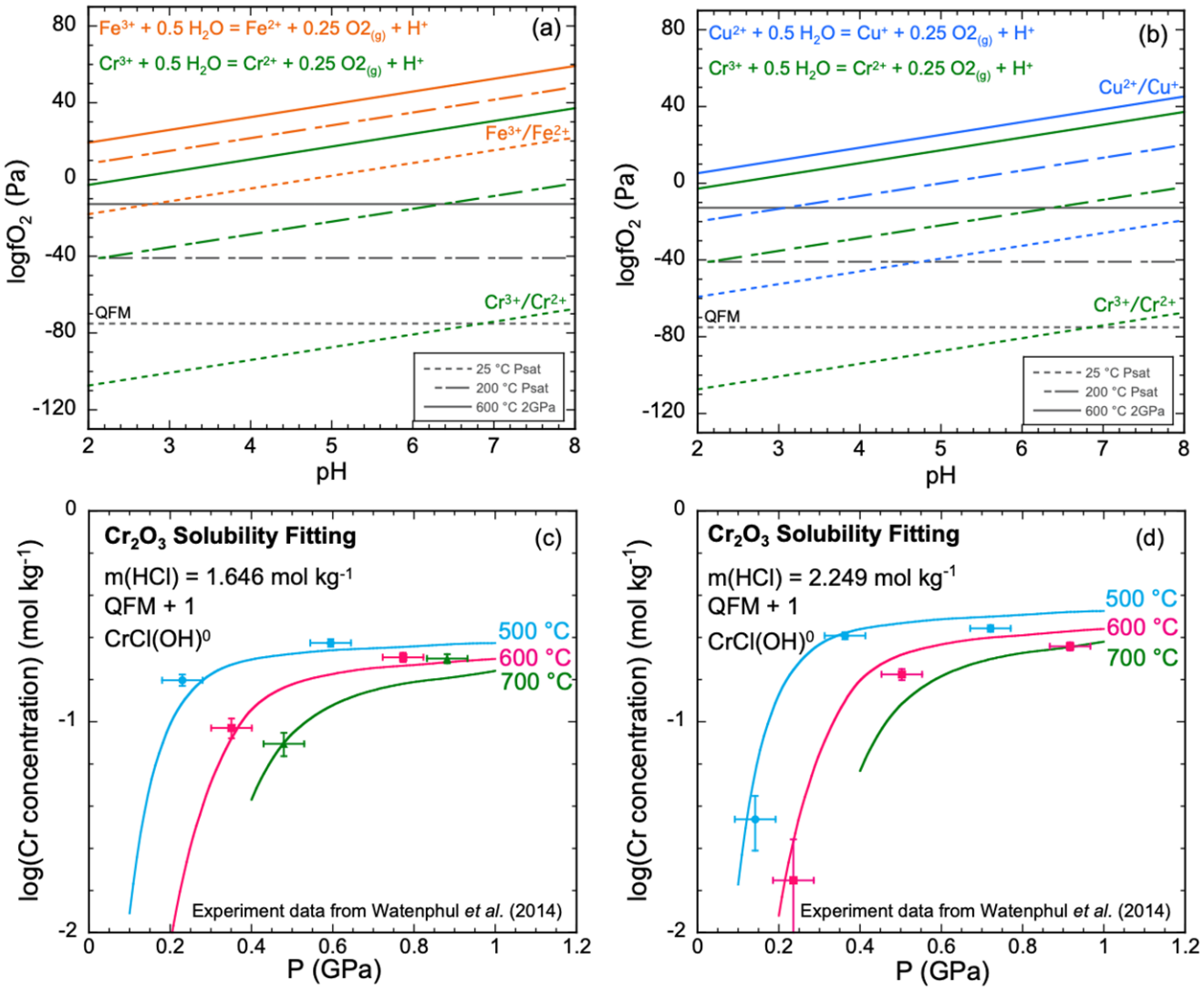

Figure 1 **(a, b)** Effect of temperature and pressure on the valence state of ions at 25 °C and Psat (dashed lines), 200 °C and Psat (dotted dashed lines) and 600 °C and 2.0 GPa (solid lines). Horizontal lines represent the QFM buffer (black): **(a)** Fe^{3+}/Fe^{2+} (orange) and Cr^{3+}/Cr^{2+} (green) **(b)** Cu^{2+}/Cu^{+} (blue) and Cr^{3+}/Cr^{2+} (green). **(c, d)** Experimental Cr_2O_3 solubilities in HCl-rich fluids at 500–700 °C and 0.1–1.0 GPa. **(c)** HCl = 1.646 mol kg^{-1}. **(d)** HCl = 2.249 mol kg^{-1}. Solid curves are fitted to the experimental data at QFM + 1.

equilibrium (Watenphul *et al.,* 2014). The horizontal error bar is the random error of pressure (±0.05 GPa). The vertical error bar is the standard error of the Cr concentration (0.01 mol kg^{-1}) calculated from the minimum detection limit of Cr (Watenphul *et al.,* 2014).

Our preliminary solubility model considered the previously estimated properties of aqueous Cr(II), (III), and (VI) species (Table S-3; Shock *et al.*, 1997; Hao, 2016). This model resulted in predicted solubilities much lower than measured. For example, at 600 °C, 1.0 GPa and 2.249 mol kg^{-1} solution, the predicted Cr concentration was 87.5 mmol kg^{-1}, about 2.6 times lower than the measured result at a similar pressure (228 mmol kg^{-1} at 0.917 GPa) (Table S-2b). Even larger discrepancies would be obtained in the KCl solutions at high pressures to be discussed below. The predominant oxidation state of the aqueous Cr was overwhelmingly +II at an oxidation state of QFM + 1 as expected by comparison with other metals. Despite the uncertainties in our overall approach, these results suggest that an additional Cr complex, probably of Cr(II), is needed to explain the high measured Cr solubilities.

The apparent importance of aqueous Cr(II) species raises the concern that there was no measurement of the oxygen fugacities for the experiments shown in Figure 1c,d. However, Watenphul *et al.* (2014) suggested that the experiments reflected oxidation states about 1.0 log unit above the QFM buffer. Under these conditions, we found that Cr(II) was the predominant valence. A second concern is the lack of experimental data for Cr speciation. However, based on *ab initio* simulations, Watenphul *et al.* (2014) suggested mixed Cr complexes with Cl, OH^-, and/or H_2O. After repeated trials of complexes such as $CrCl^+$, $Cr(OH)^+$ and $CrCl(OH)^0_2$, we found a satisfactory fit to the experimental data using the mixed complex $CrCl(OH)^0$. This complex may also have H_2O coordinated to the Cr, but we cannot determine how many with the available experimental data. Therefore, we have omitted writing them. The curves in Figure 1c,d show our best fit to the experimental data at both low and high HCl concentrations. These calculations enabled us to retrieve the log K of the dissociation reaction of $CrCl(OH)^0$ according to

$$CrCl(OH)^0 + H^+ = Cr^{2+} + Cl^- + H_2O \qquad \text{Eq. 1}$$

The retrieved log K values have an uncertainty of ±0.3 units (Table S-2a). It should be noted that retrieval of the equilibrium constant for Equation 1 was carried out with simultaneous consideration of the other aqueous Cr species mentioned above as well as species such as HCl and OH^- (SI). Because $CrCl(OH)^0$

was by far the predominant Cr species in the solubility model, the overall solubility reaction studied experimentally can be approximated by the reaction

$$Cr_2O_3 + 2Cl^- + 2H^+ = 2CrClOH^0 + 0.5O_2(g) \quad \text{Eq. 2}$$

which is a redox reaction that depends on the logfO_2 used in the calculations.

Analysis of Cr_2O_3 solubilities in KCl solutions. The only experimental data for Cr solubility at upper mantle conditions (Klein-BenDavid *et al.*, 2011) refer to the solubility of Cr_2O_3 at three KCl concentrations using the diamond trap method at 1000, 1200 °C and 4.0, 6.0 GPa. The solubilities varied with KCl concentration but did not vary significantly with temperature and pressure. Therefore, at each KCl concentration, we averaged the measurements at the different temperatures and pressures. We found that the complex $CrCl(OH)^0$ could be fitted to the data at the two highest concentrations. The data points in Figure 2 represent the experimental Cr concentrations with a standard deviation as a vertical error bar. The scatter in the experimental data precludes fitting all three data points with a single complex. However, we do not have sufficient data to justify using more than one complex. We therefore calibrated our $CrCl(OH)^0$ complex at the highest Cl concentration (Fig. 2). As a result, our predicted curve lies between the mid-KCl and low-KCl data points. The oxygen fugacity was again not controlled or measured in the experiments but was suggested to lie near to the QFM buffer. To test the sensitivity of our model calculations to the oxygen fugacity, we carried out calculations over a range of logfO_2 from QFM - 2 to QFM + 2 (Fig. 2). We subsequently used the equilibrium constant for the complex $CrCl(OH)^0$ referring to QFM + 1 for comparison with the equilibrium constants retrieved from the solubility data in Figure 1c,d. The corresponding log K values have an uncertainty of ±0.3 units (SI).

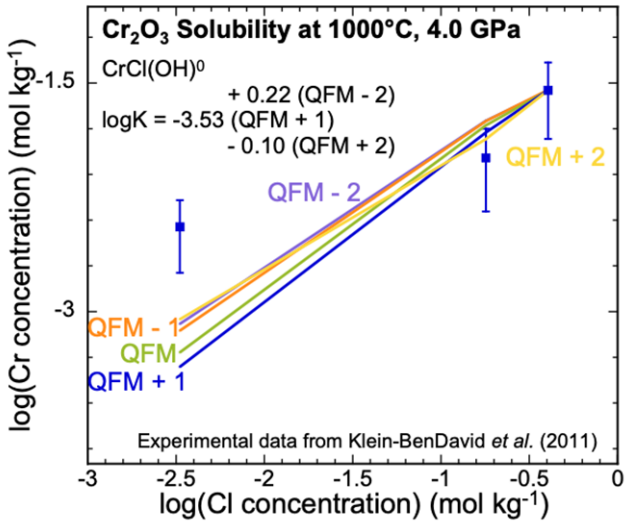

Figure 2 Experimental Cr_2O_3 solubilities in KCl fluids at 1000 °C and 4.0 GPa. Curves were fit to the highest two KCl points from QFM - 2 to QFM + 2.

Equation of state for $CrCl(OH)^0$. Assuming $CrCl(OH)^0$ was the main Cr species in both the HCl and KCl experimental fluids, we combined the values of log K retrieved from the solubility of Cr_2O_3 in HCl and KCl fluids. For the HCl experiments, each log K value shown in Figure 3 represented a fit to the trend of experimental solubilities with pressure in Figure 1 (Table S-2a). The curves in Figure 3 represent regression using the DEW model. Estimated uncertainties are on the order of ±0.3 log units. It can be seen in Figure 3a that, as expected, the $CrCl(OH)^0$ complex becomes stronger with increasing temperature and decreasing pressure, but the influence of pressure diminishes above about 2.0 GPa.

Although the curves agree within the estimated uncertainties with the experimentally calibrated log K values, it should be emphasised that the present characterisation is just a first approximation because no experimentally calibrated log K values are known below 500 °C. Nevertheless, the results serve as a valuable bridge between experiments involving Cr_2O_3 in chemically simple but different systems, *i.e.* HCl and KCl solutions, and enable extrapolation over a wide range of temperatures and pressures as shown in Figure 3b and Table S-4. We tested our model by applying it to the geochemically more complex systems of interest discussed below, some of which occur at temperatures and pressures well outside the range of calibration of the model.

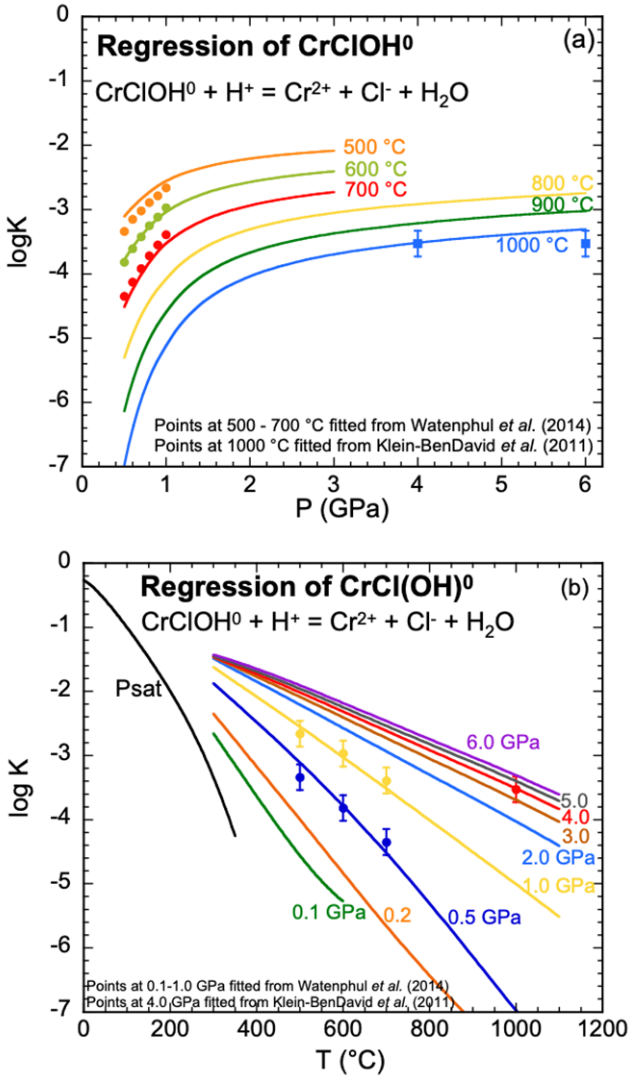

Figure 3 Regression of log K for $CrCl(OH)^0$ for dissociation reaction *versus* **(a)** pressure and **(b)** temperature up to 6.0 GPa and 1100 °C.

Predictions of Cr solubility in crustal hydrothermal and upper mantle fluids. In order to test the model, we used a range of different mineral assemblages (Table S-5) to constrain aqueous speciation and solubility model predictions of the fluid chemistry. The results (Table S-6) are not sensitive to the amounts of minerals but are sensitive to temperature, pressure and Cl concentration as discussed below. Figure 4a displays the predicted Cr solubility in five model fluids over a range of

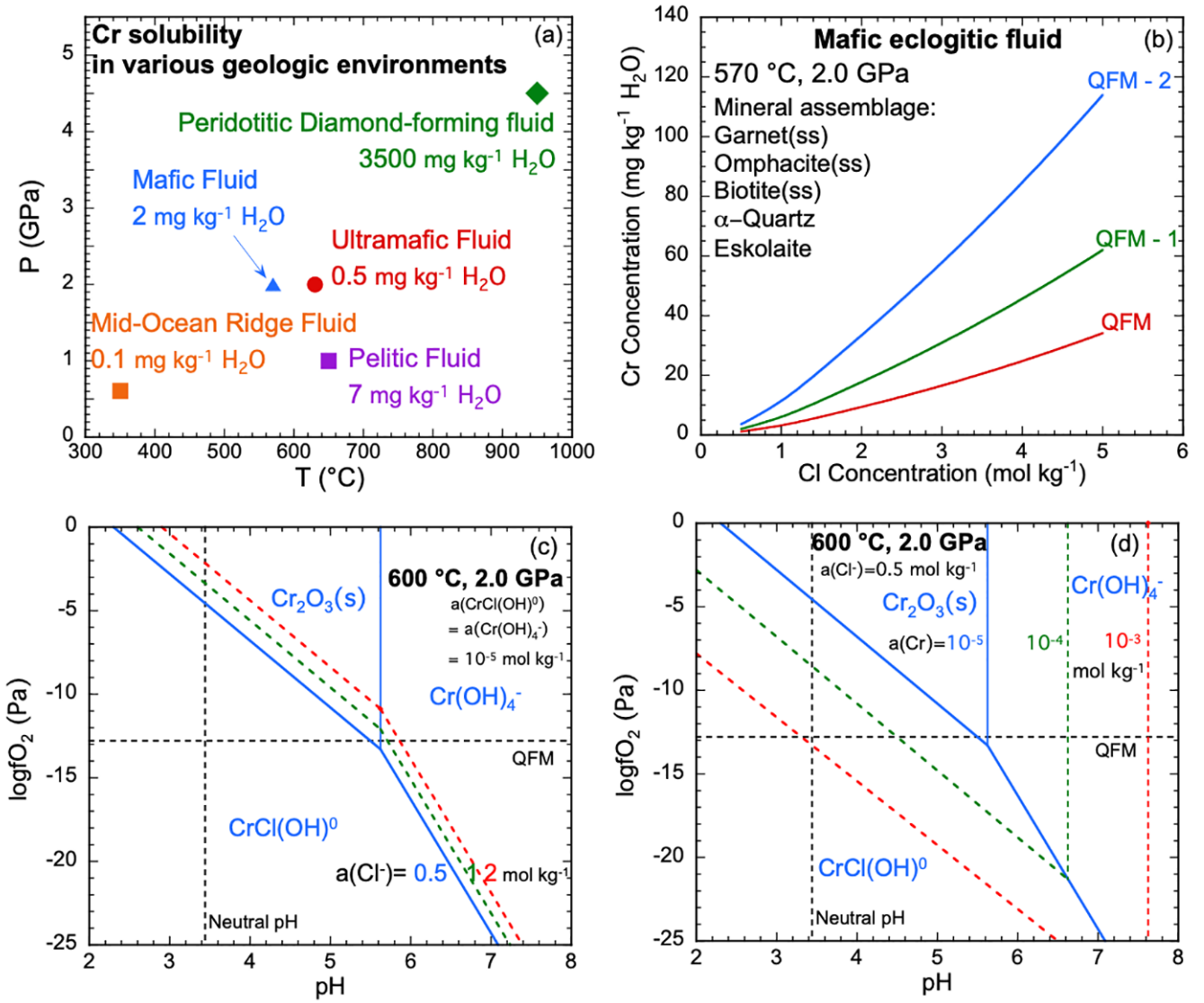

Figure 4 Prediction of Cr solubility in model fluids. **(a)** MOR, subduction zone, and diamond-forming fluids. **(b)** mafic eclogitic fluid at 570 °C and 2.0 GPa, Cr concentration *versus* Cl at QFM (red), QFM - 1 (green) and QFM - 2 (blue). Effects of Cl concentration and activity of Cr species on the solubility of $Cr_2O_3(s)$ and Cr speciation at 600 °C and 2.0 GPa: **(c)** $a(Cl^-)$ = 0.5 (solid blue), 1 (dashed green) and 2 (dashed red) mol kg^{-1}, assuming $a(CrCl(OH)^0) = a(Cr(OH)_4^-) = 10^{-5}$ mol kg^{-1}. **(d)** $a(CrCl(OH)^0) = a(Cr(OH)_4^-) = 10^{-5}$ (solid blue), 10^{-4} (dashed green), 10^{-3} (dashed red) mol kg^{-1}, when $a(Cl^-)$ = 0.5 mol kg^{-1}.

conditions: a crustal MOR fluid, pelitic, mafic, and ultramafic subduction zone fluids, and a peridotitic, diamond-forming fluid (Tomlinson *et al.*, 2006; Huang, 2017). The Cl concentrations are 0.5 mol kg^{-1}, except in the peridotitic fluid where it is 8.0 mol kg^{-1} (Huang, 2017). The ultramafic subduction zone fluid and the peridotitic fluid are in equilibrium with picrochromite, while the others are in equilibrium with eskolaite. Because these are pure minerals, the predicted solubilities are maxima. The predicted range of Cr solubilities is enormous: from 0.15 mg kg^{-1} H_2O in the MOR fluid to 3500 mg kg^{-1} H_2O in the peridotitic fluid. In all the models, $CrCl(OH)^0$ is the major Cr species.

Discussion

Crustal mid-ocean ridge (MOR) hydrothermal fluid. Prediction of the Cr content of MOR fluids is an important test of our model because the temperatures are much lower than in the experiments used to calibrate the model (Fig. 4a). At 350 °C and Psat (0.017 GPa), the MOR fluid in Figure 4a is predicted to contain only 0.1 mg kg^{-1} H_2O of Cr. The low predicted value is consistent with observations by Sander and Koschinsky (2000) who suggested that Cr was about 1200 nM (0.062 mg kg^{-1}) in their hydrothermal fluids. One difference from our prediction is that Sander and Koschinsky (2000) further suggested that hydrothermal Cr was predominantly Cr(III). However, the Cr(III) concentration was not measured directly. Instead, it was obtained from the difference between the total Cr and the Cr(VI) concentrations at ambient temperatures and pressures where Cr(III) is expected to predominate.

Subduction zone fluids. In the subduction zone fluids, the predicted Cr concentrations are 0.5, 2, and 7 mg kg^{-1} H_2O in ultramafic, mafic, and pelitic fluids, respectively. Although much higher than in the MOR fluid, Cr is still a trace element at these higher temperatures (570–650 °C) and pressures (1.0–2.0 GPa). The model ultramafic fluid has the lowest Cr because the fluid is at QFM + 2, buffered by magnetite, antigorite and chlorite (Debret and Sverjensky, 2017). The pelitic schist fluid has a higher Cr than the mafic eclogitic fluid, because the major Cr species $CrCl(OH)^0$ favours high temperature and low pressure. The strongest influences on Cr solubility are oxygen fugacity and Cl concentration.

Upper mantle peridotitic diamond-forming fluids. Cr in the peridotitic diamond-forming fluid is three orders of magnitude higher than in the other fluids. There are two reasons for this. First, the diamond-forming fluid contained 8.0 mol kg^{-1} Cl, much higher than in the other fluids. Second, the oxygen fugacity was low (QFM - 4). Although Cr was not detected in fluid inclusion studies of the Panda diamonds (Tomlinson *et al.*, 2006), our prediction of 3500 mg kg^{-1} H_2O of Cr is reasonable because it is below the detection limit of about 4000 mg kg^{-1} (Tomlinson, pers. comm.).

A comparison can also be made with an experimental study of the solubility of a mafic eclogite in Cl-free fluids (Elazar *et al.*, 2019). Chromium concentrations measured at 4.0–5.0 GPa and 900–1200 °C were 17–96 mg kg^{-1} H_2O. Our predicted Cr concentration is about 20 mg kg^{-1} H_2O with only Cr-OH complexes at 950 °C and 4.5 GPa, which is consistent with the experiments.

As already noted, Equation 2 shows that equilibrium between a Cr(III) mineral component and aqueous Cr(II) in a high temperature fluid is a redox reaction. Consequently, precipitation of a Cr(III) mineral component will also be a redox reaction. In the peridotitic, diamond-forming environment, garnet inclusions contain 3–20 wt. % Cr_2O_3 (Stachel and Harris, 2008). A possible redox reaction that could account for such garnets might be

$$Mg_3Al_2Si_3O_{12} + 2Mg_2SiO_4 + 4CrCl(OH)^0 + H_2CO_3^0 + SiO_2(aq) \rightarrow 2Mg_3Cr_2Si_3O_{12} + MgAl_2O_4 + C(diamond) + 4Cl^- + 4H^+ + H_2O \quad \text{Eq. 3}$$

where $H_2CO_3^0$ is reduced to C (diamond) while Cr(II) is oxidised to Cr(III).

Can Cr be more soluble in subduction zone fluids? To investigate further the factors influencing Cr solubility, Figure 4b presents the predicted Cr concentrations at 570 °C and 2.0 GPa in the mafic fluid as a function of Cl concentration and oxygen fugacity. At QFM and with Cl increasing from 0.5 mol kg^{-1} to 5.0 mol kg^{-1}, the Cr solubility increases up to 34 mg kg^{-1} H_2O, about a 30-fold increase. The increase at QFM - 2 with Cl is even more dramatic. These results suggest that mafic fluids could transport large concentrations of Cr at Cl-rich or reducing conditions. Such concentrations of Cr are consistent with a metasomatic origin for the occurrence of Cr-rich pyroxene in eclogitic veins in a metagabbro complex (Spandler *et al.*, 2011).

In the mafic eclogitic fluid, we tested the Cr solubility with no Cl and found a Cr solubility of 0.06 mg kg^{-1} H_2O, much lower than the original prediction when Cl was 0.5 mol kg^{-1}. The major Cr species is $Cr(OH)_4^-$. Therefore, we explored the effect of Cl concentration and activity of $CrCl(OH)^0$ and $Cr(OH)_4^-$ on Cr_2O_3 dissolution, presented in Figure 4c,d as diagrams of logfO_2 *versus* pH. It can be seen that the stability field of $CrCl(OH)^0$ expands with increasing Cl concentration and total Cr in the fluids. As mentioned above, elements tend to occur with lower valence state with increasing temperature. Figure 1a,b show that ions of Fe, Cu and Cr obey this trend. Although the stability field of Cr^{2+} is very small at 25 °C and Psat, at 600 °C and 2.0 GPa, Cr^{2+} is stable above QFM at most pH values.

Conclusions

The model presented here provides a framework for assessing the mobility of Cr in deep crustal and upper mantle fluids. Predicted chromium solubilities range widely. In MOR fluids Cr is almost insoluble. However, Cr can be highly soluble in reducing, Cl-bearing, subduction zone fluids. High predicted Cr concentrations in a peridotitic, diamond-forming fluid imply that Cr could be involved in the formation of diamond and Cr(III) garnet *via* a redox reaction. Chromium in the fluid could be oxidised and incorporated into garnet while C is reduced and precipitated as diamond. Such a redox reaction would explain the strong geologic linkage between diamonds and Cr-rich garnets.

Acknowledgements

Research was supported by the Johns Hopkins University, the Deep Carbon Observatory, the National Science Foundation, and the Department of Energy.

Editor: Horst R. Marschall

Additional Information

Supplementary Information accompanies this letter at http://www.geochemicalperspectivesletters.org/article1926.

Cite this letter as: Huang, J., Hao, J., Huang, F., Sverjensky, D.A. (2019) Mobility of chromium in high temperature crustal and upper mantle fluids. *Geochem. Persp. Let.* 12, 1–6.

References

Akizawa, N., Tamura, A., Fukushi, K., Yamamoto, J., Mizukami, T., Python, M., Arai, S. (2016) High-temperature hydrothermal activities around suboceanic Moho: An example from diopsidite and anorthosite in Wadi Fizh, Oman ophiolite. *Lithos* 263, 66–87.

Debret, B., Sverjensky, D.A. (2017) Highly oxidising fluids generated during serpentinite breakdown in subduction zones. *Scientific Reports* 7, 10351.

Elazar, O., Frost, D., Navon, O., Kessel, R. (2019) Melting of hydrous carbonated eclogite at 4-6 GPa and 900-1200°C: implications for the generation of diamond-forming fluids. *Geochimica et Cosmochimica Acta* 255, 69–87.

Hao, J. (2016) Geochemical signatures of weathering and surface water chemistry in the late Archean. PhD thesis, Johns Hopkins University, 248 pp.

Huang, F. (2017) Evolution of aqueous fluids, hydrocarbons, and diamond formation in the upper mantle. PhD thesis, Johns Hopkins University, 207 pp.

Johan, Z., Martin, R.F., Ettler, V. (2017) Fluids are bound to be involved in the formation of ophiolitic chromite deposits. *European Journal of Mineralogy* 29, 543–555.

Klein-BenDavid Ofra, O., Pettke, T., Kessel, R. (2011) Chromium mobility in hydrous fluids at upper mantle conditions. *Lithos* 125, 122–130.

Mei, Y., Sherman, D.M., Liu, W., Brugger, J. (2013) Ab initio molecular dynamics simulation and free energy exploration of copper(I) complexation by chloride and bisulfide in hydrothermal fluids. *Geochimica et Cosmochimica Acta* 102, 45–64.

Rai, D., Sass, B.M., Moore, D.A. (1987) Chromium (III) hydrolysis constants and solubility of chromium (III) hydroxide. *Inorganic Chemistry* 26, 345–349.

Saleh, F.Y., Parkerton, T.F., Lewis, R.V., Huang, J.H., Dickson, K.L. (1989) Kinetics of chromium transformations in the environment. *Science of the Total Environment* 86, 25–41.

Sander, S., Koschinsky, A. (2000) Onboard-ship redox speciation of chromium in diffuse hydrothermal fluids from the North Fiji Basin. *Marine Chemistry* 71, 83–102.

Shock, E.L., Sassani, D.C., Willis, M., Sverjensky, D.A. (1997) Inorganic species in geologic fluids: Correlations among standard molal thermodynamic properties of aqueous ions and hydroxide complexes. *Geochimica et Cosmochimica Acta* 61, 907–950.

Spandler, C., Pettke, T., Rubatto, D. (2011) Internal and external fluid sources for eclogite-facies veins in the Monviso Meta-ophiolite, Western Alps: Implications for fluid flow in subduction zones. *Journal of Petrology* 52, 1207–1236.

Stachel, T., Harris, J.W. (2008) The origin of cratonic diamonds - Constraints from mineral inclusions. *Ore Geology Reviews* 34, 5–32.

Sverjensky, D.A. (1984) Europium redox equilibria in aqueous solution. *Earth and Planetary Science Letters* 67, 70–78.

Sverjensky, D.A., Harrison, B., Azzolini, D. (2014). Water in the deep Earth: the dielectric constant and the solubilities of quartz and corundum to 60 kb and 1200 C. *Geochimica et Cosmochimica Acta, 129,* 125–145.

Testemale, D., Brugger, J., Liu, W., Etschmann, B., Hazemann, J.L. (2009) In-situ X-ray absorption study of Iron(II) speciation in brines up to supercritical conditions. *Chemical Geology* 264, 295–310.

Tomlinson, E.L., Jones, A.P., Harris, J.W. (2006) Co-existing fluid and silicate inclusions in mantle diamond. *Earth and Planetary Science Letters* 250, 581–595.

Watenphul, A., Schmidt, C., Jahn, S. (2014) Cr(III) solubility in aqueous fluids at high pressures and temperatures. *Geochimica et Cosmochimica Acta* 126, 212–227.

Zemniak, S.E., Jones, M.E., Combs, K.E.S. (1998) Solubility and phase behavior of Cr(III) oxides in alkaline media at elevated temperatures. *Journal of Solution Chemistry* 27, 33–66

Geochemical Perspectives Letters

Mobility of chromium in high-temperature crustal and upper mantle fluids

J. Huang, J. Hao, F. Huang, D.A. Sverjensky

Supplementary Information

The Supplementary Information includes:

- Theoretical Approaches
- Uncertainties in the Regression of the Experimental Data
- Fluid Models for Prediction of Cr Solutions
- Tables S-1 to S-6
- Figures S-1 and S-5
- Supplementary Information References

Theoretical approaches

To calculate the solubility of Cr in deep Earth fluids, we need the equilibrium constants of reactions involving Cr-minerals and Cr aqueous species. Therefore, the thermodynamic properties of each Cr mineral and aqueous species are essential.

For Cr-minerals we focused on eskolaite (Cr_2O_3) and picrochromite ($MgCr_2O_4$) because these are the best characterized by experimental studies and because the experimental solubilities we analyzed refer to measurements of the solubility of eskolaite. The Gibbs free energies of formation for the Cr minerals as functions of temperature and pressure were calculated using SUPCRT92b, a version of SUPCRT92 (Johnson *et al.*, 1992) based on data for minerals from Berman (1988) and Sverjensky *et al.* (1991). The thermodynamic properties of eskolaite and picrochromite are listed in Table S-1. For Cr_2O_3, the calorimetric $\Delta H^0_{f;\,Pr,Tr}$ (Klemme *et al.*, 2000) is directly used because this mineral is a pure Cr oxide endmember, its properties do not depend on those of non-Cr minerals. The heat capacities for Cr_2O_3 published by various experiments (Klemme *et al.*, 2000 and Ziemiak *et al.* 2007) showed a lambda peak transition at 305.5 K. We fitted this transition using the empirical formula from Berman and Brown (1985) (Fig. S-1). The parameters of volume were fitted based on experimental data (Dymshits *et al.*, 2016), presented in Fig. S-2.

For $MgCr_2O_4$, we also fitted the parameters of heat capacity and volume based on previous experimental data, presented as curves in Figures S-3 and S-4. Due to a lack of calorimetric experiments, the $\Delta G^0_{f;\,Pr,Tr}$ for $MgCr_2O_4$ was retrieved from the equilibrium reaction

$$MgSiO_3 + Cr_2O_3 = MgCr_2O_4 + SiO_2 \qquad \text{Eq. S-1}$$

using the thermodynamic properties of $MgSiO_3$ and SiO_2 from Berman (1988) and Cr_2O_3 obtained above (Fig. S-5).

The regression of the experimental solubility data for Cr_2O_3 was carried out to obtain values of the equilibrium constant (log K) of the $CrCl(OH)^0$ complex using EQ3, which is a theoretical code simulating water-rock equations at upper mantle conditions modified from the code published by Wolery (1983, 1992). The equation of state coefficients and standard partial molal properties for the complex $CrCl(OH)^0$ were obtained by regression using the Deep Earth Water (DEW) model to obtain the ΔG_f^0, S^0, V^0, Cp and $\omega \times 10^{-5}$ and correlation coefficients a1, a2, a3, a4, c1, and c2 of the revised Helgeson-Kirkham-Flowers equations (Helgeson *et al.*, 1981; Shock and Helgeson, 1988). In our EQ3 and DEW database, the equations of state for Cr^{3+} and Cr^{2+} were included from Hao (2016), as well as the complexes $CrCl^{2+}$, $HCrO_4^-$, CrO_4^{2-}, $Cr_2O_7^{2-}$. The thermodynamic properties of the complex $CrCl(OH)^0$ are listed in Table S-3, along with other preliminary Cr-Cl and Cr-OH complexes. Also, given are the predicted log K values extrapolated over a wide range of temperatures and pressures (Table S-4).

Uncertainties in the regression of the experimental data

The uncertainties in our values of log K obtained by regression of experimental solubilities results from experimental uncertainties and assumptions during the regression procedure. One key assumption during the regression calculations involves the $logfO_2$. In both the HCl and the KCl experiments (Watenphul *et al.*, 2014 and Klein-BenDavid *et al.*, 2011), the $logfO_2$ and pH were not directly measured. In the Deep Earth Water model, pH can be calculated by providing initial chemical compositions, mineral assemblages and the $log\ fO_2$ in the input file. However, there are suggestions about the $logfO_2$ in both experimental studies. First, the $logfO_2$ of HCl solutions (Watenphul *et al.*, 2014) was recommended as reducing but above the QFM buffer. Therefore, QFM+1 was chosen as the value of the $logfO_2$ in our models. To test the sensitivity of our log K values in response to a one-unit change of $logfO_2$, we calculated the change of log K of the complex $CrCl(OH)^0$ at 600 °C. The deviation of log K was ±0.20 and ±0.25 at 0.2 GPa and 1.0 GPa, representatively. The complex $CrCl(OH)^0$ is the dominant species between QFM and QFM+2. Second, the $logfO_2$ of KCl solutions were suggested to be near the QFM buffer. We regressed the log K of the complex $CrCl(OH)^0$ at 1000 °C and 4.0 GPa from QFM -2 to QFM +2 by fitting the points with the two highest Cl concentrations (Fig. 2), ranging from -3.31 to -3.63, with uncertainties up to +0.22. The log K of -3.53 at QFM+1 was selected for consistency with the former experiments. At the lowest Cl concentration, the predicted solubility is lower than the data, suggesting the complex $CrCl(OH)^0$ is not sufficiently important at very low Cl concentrations. There are insufficient data to characterize an additional Cr complex at those low Cl concentrations. The overall uncertainty of the regressed log K for the complex $CrCl(OH)^0$ is estimated to be ±0.3 units (Sverjensky *et al.*, 2014).

Fluid models for Prediction of Cr Solubilities

The predictions of Cr solubility in different geological environments were made using the aqueous speciation-solubility code EQ3. Fluids in three geologic settings were modelled: a mid-ocean ridge (MOR) fluid, three subduction zone fluids and a peridotitic diamond-forming fluid. For the subduction zone fluids, the predictions are applied to three types of mineral assemblages: pelitic, mafic, and ultramafic. The fluid models above were constrained by the specific mineral assemblages and conditions summarized in Table S-5.

The results of the fluid models are given as molalities of the elements and percentages of the principal aqueous species in Table S-6. The chemical compositions of fluids in different geological settings vary widely. The MOR fluid is the most dilute, because it represents altered seawater. The three subduction zone fluids have similar K concentrations. The pelitic and mafic fluids are similar in Na, Ca, Mg, Si and Fe, but lower than Al in the pelitic fluid. The pelitic fluid has the highest Cr among the subduction zone fluids because of its higher temperature but lower pressure and lower $logfO_2$ than the ultramafic fluid. The ultramafic fluid is special because it has the lowest Na, Ca, Al, Si, Fe but the highest Mg, compared with the pelitic and mafic fluids. The Cr solubility is low in the ultramafic fluid because the $logfO_2$ is buffered by the mineral assemblage antigorite, magnetite and clinochlore. The peridotitic diamond-forming fluid has the highest salinity (Cl = 8.0 mol kg^{-1}) and the highest solubilities of elements (except Mg) at 950 °C and 4.5 GPa. Therefore, the Cr solubility is remarkably high. High solubility of C exists in this fluid because of equilibrium with diamond.

The characteristics and percentage of aqueous species are various in different fluids. The complex $CrCl(OH)^0$ is the major aqueous species for Cr in every fluid. The major complexes of each other element in the MOR fluid is the simplest with only Cl ligands. In subduction zone and peridotitic fluids, silicate complexes are important, especially mixed Mg complex $Mg(SiO_2)HCO_3^+$, and Al complex $Al(OH)_3OSi(OH)_3^-$. In peridotitic fluid, aqueous organic species of methane, ethane and propane are major C species.

Supplementary Tables

Table S-1 Thermodynamic properties of Cr_2O_3 and $MgCr_2O_4$.

Mineral	ΔG_f^0 [a]	ΔH_f^0 [a]	S^0 [b]	Cp [b]	K_0 [d]	K_1 [d]	K_2 [d]	K_3 [d]
Cr_2O_3	-1,046.2[f]	-1,128.2[f]	83.8[f]	98.0[g]	139.6[g]	-501.4[g]	-1,340,000[g]	67,420,000[g]
$MgCr_2O_4$	-1,655.8[j]	-1,769.2	113.1[j]	129.0[k]	220.5[k]	-1245[k]	-2,658,000[k]	210,400,000[k]

Mineral	T_{lambda} [d]	T_{ref} [d]	l_1	l_2
Cr_2O_3	305.5[g]	298.15	-11.23 [g]	0.03676 [g]

Mineral	V^0 [c]	$v_1 \times 10^5$ [e]	$v_2 \times 10^5$ [e]	$v_3 \times 10^5$ [e]	$v_4 \times 10^8$ [e]
Cr_2O_3	29.09[h]	2.861[i]	-3.527×10^{-4} [i]	-0.05182 [i]	4.888×10^{-5} [i]
$MgCr_2O_4$	43.58[l]	1.607[m]	2.131×10^{-4} [m]	-0.05034[n]	3.513×10^{-5} [n]

[a] $kJ \cdot mole^{-1}$; [b] $J \cdot mole^{-1} \cdot K^{-1}$; [c] $cm^3 \cdot mole^{-1}$; [d]equation from Berman and Brown (1985); $Cp = k_0 + k_1 \times T^{-0.5} + k_2 \times T^{-2} + k_3 \times T^{-3} + Cp_\lambda$, when a lambda transition of the mineral at T_{lambda}, for $T_{ref} \leq T \leq T_\lambda$, $Cp_\lambda = T(l_1 + l_2 T)^2$; [e]$V = V^0[1 + v_1(T - 298) + v_2(T - 298)^2 + v_3(P - 1) + v_4(P - 1)^2]$; where T in K and P in bar; [f]calorimetric ΔH_f^0 and S from Klemme *et al*. (2000); [g]Cp parameters fitted from Klemme *et al*. (2000) and Ziemniak *et al*. (2007); [h]Holland and Powell (2011); [i]extrapolated from Dymshits *et al*. (2016); [j]retrieved from Klemme and O'Neill (1997); [k]Cp parameters fitted from Klemme *et al*. (2000) and Naylor (1944); [l]O'Neill and Dollase (1994); [m]fitted from Kaprálik (1969); [n]fitted from Nestola *et al*. (2014).

Table S-2 **(a)** log K values of $CrCl(OH)^0$ retrieved from Watenphul *et al*. (2014). Numbers in parenthesis have large uncertainties.

log K		T (°C)		
		500	600	700
P (GPa)	0.1	(-4.2)		
	0.2	(-4.1)	(-4.3)	
	0.3	(-3.9)	(-4.2)	
	0.4	(-3.6)	(-4.1)	(-4.5)
	0.5	-3.3	-3.8	-4.4
	0.6	-3.2	-3.6	-4.1
	0.7	-3.0	-3.4	-3.9
	0.8	-2.9	-3.3	-3.7
	0.9	-2.8	-3.1	-3.6
	1.0	-2.7	-3.0	-3.4

(b) Comparison of Cr_2O_3 solubility in experimental 2.249 mol kg^{-1} HCl fluids and alternate speciation models with only Cr ions, with Cr-Cl complexes, and with $CrCl(OH)^0$. Cr concentrations are in mmol kg^{-1} H_2O.

Experiment: 0.363 GPa, 500 °C; Cr = 256 mmol kg^{-1} H_2O Models:		
0.4 GPa, 500 °C	Cr solubility	Cr speciation
Only ions	1.73	Cr^{2+}(94), Cr^{3+}(6)
Cl complex	107	$CrCl_2^0$(43), $CrCl^+$(40), $CrCl_2^+$(10), $CrCl^{2+}$(6), Cr^{2+}(1)
$CrCl(OH)^0$	277	$CrCl(OH)^0$(100)

Experiment: 0.917 GPa, 600 °C; Cr = 228 mmol kg^{-1} H_2O Models:		
1.0 GPa, 600 °C	Cr solubility	Cr speciation
Only ions	3.36	Cr^{2+}(98), Cr^{3+}(2)
Cl complex	87.5	$CrCl^+$(59), $CrCl_2^0$(22), $CrCl^{2+}$(9), $CrCl_2^+$(8), Cr^{2+}(2)
$CrCl(OH)^0$	276	$CrCl(OH)^0$(100)

Table S-3 Thermodynamic properties of $CrCl(OH)^0$ and other Cr aqueous species in the DEW model from preliminary studies.

(a) Values using the units in the Deep Earth Water model.

Cr aqueous species		ΔG_f^0 [a]	ΔH_f^0 [a]	S^0 [b]	Cp [b]	V^0 [c]	$\omega \times 10^{-5}$ [a]	$a_1 \times 10$ [d]	$a_2 \times 10^{-2}$ [a]	a_3 [e]	$a_4 \times 10^{-4}$ [f]	c_1 [b]	$c_2 \times 10^{-4}$ [f]
Cr(II)	Cr^{2+}	-36,600[g]	-34,400[g]	-19.0[g]	-4.4[h]	-17.0[h]	1.35i	0.262	-9.00	8.76	-2.41	16.0	-3.93
	$CrOH^+$	-84,300[j]	-96,900	-12.1j	9.7[h]	-12.0[h]	0.73	-0.458	-4.72	8.79	-2.58	18.6	-1.06
	$CrCl^+$	-69,180[k]	-74,700	-1.74[l]	24[l]	7.8[l]	0.58	3.31	-1.13	5.79	-2.73	25.6	1.85
	$CrCl_2^0$	-100,300[k]	-115,800	7.11[l]	42.6[l]	35.4[l]	-0.038	8.38	3.69	1.74	-2.93	30.8	5.64
	$CrCl(OH)^0$	-125,200	-140,239	22.0	28.6	35.0	0.30	7.22	2.60	2.67	-2.89	29.4	4.09
Cr(III)	Cr^{3+}	-45,700[g]	-55,000[g]	-71.9[g]	-24.0[h]	-40.0[h]	2.67	-7.36	-2.80	13.4	-2.67	16.7	-7.92
	$CrOH^{2+}$	-97,200[m]	-113,800	-41.0[n]	9.5[h]	-25.7[o]	1.01	-2.67	-6.82	10.6	-2.50	27.2	-1.09
	$Cr(OH)_2^+$	-144,000[m]	-173,900	-30.1[p]	10.7[h]	-15[h]	1.01	-0.91	-5.15	9.16	-2.57	21.7	-0.86
	$CrOH_3^0$	-194,600[q]	-232,500	-0.90[q]	34[h]	3.8[h]	-0.038	2.23	-2.16	6.65	-2.69	25.7	3.89
	$CrOH_4^-$	-233,600[q]	-280,400	24.8[q]	19.3[h]	26.7[h]	1.25	7.31	2.67	2.60	-2.89	29.0	0.90
	$CrCl^{2+}$	-76,100[m]	-89,800	-45.0[p]	-2.1[r]	-17.8[l]	1.74	-1.10	-5.33	9.31	-2.56	21.0	-3.46
	$CrCl_2^+$	-106,100[m]	-122,300	-11.0[p]	-0.3[s]	6.9[l]	0.72	3.21	-1.23	5.87	-2.73	12.6	-3.10
Cr(VI)	$HCrO_4^{2-}$	-183,700[t]	-210,000[t]	46.6[t]	1.5[t]	44.9[t]	-0.963	10.7	5.90	-0.114	-3.02	15.9	-2.73
	CrO_4^{2-}	-174,800[t]	-210,930[t]	13.8[t]	-62.6[t]	19.8[t]	3.00	10.0	-6.21	1.65	-2.52	-2.86	-15.8
	$Cr_2O_7^{2-}$	-312,970[t]	-355,370 [t]	72.0[t]	-29.1[t]	72.7[t]	2.27	16.7	11.6	-4.92	-3.26	9.98	-8.96

[a] $cal \cdot mole^{-1}$; [b] $cal \cdot mole^{-1} \cdot K^{-1}$; [c] $cm^3 \cdot mole^{-1}$; [d] $cal \cdot mole^{-1} \cdot bar^{-1}$; [e] $cal \cdot K \cdot mole^{-1} \cdot bar^{-1}$; [f] $cal \cdot K \cdot mole^{-1}$. [g]Johnson and Nelson (2012); [h]calculated from the given values of S with the equations proposed by Shock *et al.*, (1997); [i]calculated from enthalpy of the complexation reaction by Dellien and Hepler (1976); [j]Slobodov *et al.* (1993); [k]calculated by assuming log β($CrCl^+$) = log β($CuCl^+$) = 0.876, log β($CrCl_{2,aq}$) = log β($CuCl_{2,aq}$) = 0.653 (Meng and Bard, 2015); [l]estimated with equations from Sverjensky *et al.* (1997); [m]calculated using the log K values recommended by Dellien *et al.* (1976); [n]ΔS_r from Baes and Mesmer (1981), originally from Postmus and King (1955); [o]Asano and Le Noble (1978); [p]calculated using ΔG_r, ΔH_r, or ΔS_r from Dellien *et al.* (1976); [q]calculated using ΔG_r and ΔS_r from Ziemniak *et al.* (1998); [r]estimated by assuming $\Delta C_{p,r} = 0$ for the reaction: $Cr^{3+} + FeCl^{2+} \rightarrow CrCl^{2+} + Fe^{3+}$; [s]estimated by assuming $\Delta C_{p,r} = 0$ for the reaction: $CrCl^{2+} + FeCl_2^+ \rightarrow CrCl_2^+ + FeCl^{2+}$; [t]Shock *et al.* (1997); [u]Accornero *et al.* (2010).

(b) Values using the SI units.

Cr aqueous species		ΔG_f^0 [a]	ΔH_f^0 [a]	S^0 [b]	Cp [b]	V^0 [c]	$\omega \times 10^{-5}$ [a]	$a_1 \times 10$ [d]	$a_2 \times 10^{-2}$ [a]	a_3 [e]	$a_4 \times 10^{-4}$ [f]	c_1 [b]	$c_2 \times 10^{-4}$ [f]
Cr(II)	Cr^{2+}	-153.1	-143.9	-79.5	-18.4	-17.0	5.65	1.10	-37.7	36.7	-10.1	66.9	-16.4
	$CrOH^+$	-352.7	-405.4	-50.6	40.6	-12.0	3.05	-1.92	-19.7	36.8	-10.8	77.8	-4.40
	$CrCl^+$	-289.4	-312.5	-7.28	100	7.80	2.43	13.9	-4.70	24.2	-11.4	107	7.70
	$CrCl_2^0$	-419.7	-484.5	29.8	178	35.4	-0.160	35.1	15.4	7.30	-12.3	129	23.6
	$CrCl(OH)^0$	-523.8	-586.8	92.1	120	35.0	1.26	30.2	10.9	11.2	-12.1	123	17.1
Cr(III)	Cr^{3+}	-191.2	-230.1	-301	-100	-40.0	11.2	-30.8	-11.7	56.1	-11.2	69.9	-33.1
	$CrOH^{2+}$	-406.7	-476.1	-172	39.8	-25.7	4.23	-11.2	-28.5	44.4	-10.5	114	-4.60
	$Cr(OH)_2^+$	-602.5	-727.6	-126	44.8	-15.0	4.23	-3.81	-21.5	38.3	-10.8	90.8	-3.60
	$CrOH_3^0$	-814.2	-972.8	-3.77	142	3.80	-0.160	9.33	-9.00	27.8	-11.3	108	16.3
	$CrOH_4^-$	-977.4	-1173	104	80.8	26.7	5.23	30.6	11.2	10.9	-12.1	121	3.80
	$CrCl^{2+}$	-318.4	-375.7	-188	-8.79	-17.8	7.28	-4.60	-22.3	39.0	-10.7	87.9	-14.5
	$CrCl_2^+$	-443.9	-511.7	-46.0	-1.26	6.90	3.01	13.4	-5.10	24.6	-11.4	52.7	-13.0
Cr(VI)	$HCrO_4^{2-}$	-768.6	-878.6	195	6.28	44.9	-4.03	44.8	24.7	-0.500	-12.6	66.5	-11.4
	CrO_4^{2-}	-731.4	-882.5	57.7	-262	19.8	12.6	41.8	-26.0	6.90	-10.5	-12.0	-66.1
	$Cr_2O_7^{2-}$	-1310	-1487	301	-122	72.7	9.50	69.9	48.5	-20.6	-13.6	41.8	-37.5

[a] $kJ \cdot mole^{-1}$; [b] $J \cdot mole^{-1} \cdot K^{-1}$; [c] $\times 10^{-6}\ m^3 \cdot mole^{-1}$; [d] $\times 10^{-5}\ J \cdot mole^{-1} \cdot Pa^{-1}$; [e] $\times 10^{-5}\ J \cdot K \cdot mole^{-1} \cdot Pa^{-1}$; [f] $J \cdot K \cdot mole^{-1}$.

Table S-4 Predicted log K of dissociation reaction for $CrCl(OH)^0$.

log K		P (GPa)						
		0.5	1.0	2.0	3.0	4.0	5.0	6.0
T (°C)	300	-1.9	-1.6	-1.5	-1.5	-1.5	-1.5	-1.4
	350	-2.2	-1.9	-1.7	-1.6	-1.6	-1.6	-1.5
	400	-2.5	-2.1	-1.8	-1.8	-1.7	-1.7	-1.6
	450	-2.8	-2.3	-2.0	-1.9	-1.9	-1.8	-1.8
	500	-3.1	-2.5	-2.2	-2.1	-2.0	-2.0	-1.9
	550	-3.4	-2.8	-2.4	-2.2	-2.2	-2.1	-2.0
	600	-3.8	-3.0	-2.6	-2.4	-2.3	-2.2	-2.2
	650	-4.1	-3.3	-2.8	-2.6	-2.5	-2.4	-2.3
	700	-4.5	-3.5	-2.9	-2.7	-2.6	-2.5	-2.5
	750	-4.9	-3.8	-3.1	-2.9	-2.8	-2.7	-2.6
	800	-5.3	-4.0	-3.3	-3.1	-2.9	-2.8	-2.7
	850	-5.7	-4.3	-3.5	-3.2	-3.1	-3.0	-2.9
	900	-6.1	-4.5	-3.7	-3.4	-3.2	-3.1	-3.0
	950	-6.6	-4.8	-3.8	-3.5	-3.4	-3.3	-3.2
	1000	-7.0	-5.0	-4.0	-3.7	-3.5	-3.4	-3.3
	1050	-7.4	-5.3	-4.2	-3.9	-3.7	-3.6	-3.5
	1100	-7.8	-5.5	-4.4	-4.0	-3.8	-3.7	-3.6

Table S-5 Characteristics of model crustal and upper mantle fluids for predicting Cr solubilities.

Type of fluids	T	P	$logfO_2$	Cl	Mineral assemblage
Mid-Ocean Ridge	350	Psat 0.017	-25.2 (Pa)	0.49	talc, clinochlore, quartz, magnetite, and eskolaite
Pelitic schist	650	1.0	QFM	0.5	plagioclase(ss): albite (53), anorthite (47); biotite(ss): phlogopite (88), annite (12); muscovite, kyanite, quartz, and eskolaite
Mafic eclogitic	570	2.0	QFM-1	0.5	garnet(ss): pyrope (12), almandine (63), grossular (25); omphacite(ss): diopside (32), hedenbergite (26), jadeite (42); quartz, and eskolaite
Ultramafic antigorite	630	2.0	QFM+2	0.6	antigorite, magnetite, clinochlore, and picrochromite
Peridotitic diamond	950	4.5	QFM-4	8.0	garnet(ss): pyrope (69), almandine (15), grossular (16); olivine(ss):forsterite (92), fayalite (8); orthopyroxene(ss): enstatite-or (91), ferrosilite (9); phlogopite, diamond, and picrochromite

Temperature in °C, pressure in GPa and Cl in $mol\ kg^{-1}$.

Source of fluid models: mid-ocean ridge mineral assemblage based on a speciation solubility model of the chemical analysis reported by Von Damm (1990); pelitic mineral assemblage represents a hypothetical pelitic schist; mafic mineral assemblage based on Viete *et al.* (2018); ultramafic mineral assemblage from Debret and Sverjensky (2017); peridotitic mineral assemblage from Huang (2017).

Table S-6 Solubilities (**a – c**) and speciation (**d – f**) of model crustal and upper mantle fluids. The unit of solubilities of elements is mmol kg^{-1} H_2O. The numbers in parentheses represent the percentages of each aqueous species of a given chemical element.

(a)	350 °C, Psat (0.017 GPa)
ELEMENT	Mid-ocean ridge
Na	$4.3*10^{-1}$
K	$2.5*10^{-2}$
Ca	$1.0*10^{-2}$
Mg	$2.6*10^{-3}$
Al	$8.8*10^{-7}$
Si	$1.3*10^{-2}$
Fe	$1.8*10^{-3}$
Zn	$1.1*10^{-4}$
Pb	$4.8*10^{-7}$
S	$2.3*10^{-3}$
C	$4.7*10^{-3}$
Cr	2.8*10-6
log$f$O2 (Pa)	-25.2
ΔQFM	+1.8
pH	4.79
a_{H_2O}	0.99

(b)	650 °C, 1.0 GPa	570 °C, 2.0 GPa	630°C, 2.0 GPa
ELEMENT	Pelitic Schist	Eclogitic mafic	Antigorite ultramafic
Na	$3.5*10^{-1}$	$4.1*10^{-1}$	$1.4*10^{-1}$
K	$7.7*10^{-2}$	$1.0*10^{-1}$	$1.0*10^{-1}$
Ca	$1.9*10^{-2}$	$1.9*10^{-2}$	$1.0*10^{-3}$
Mg	$4.5*10^{-2}$	$3.0*10^{-2}$	$6.6*10^{-1}$
Al	$9.1*10^{-3}$	$2.5*10^{-2}$	$5.1*10^{-4}$
Si	$5.7*10^{-1}$	$5.3*10^{-1}$	$4.5*10^{-1}$
Fe	$6.5*10^{-2}$	$7.0*10^{-2}$	$3.5*10^{-2}$
C	1.0	1.0	1.0
Cr	$1.1*10^{-4}$	$3.9*10^{-5}$	$9.8*10^{-6}$
log$f$O2 (Pa)	-12.3	-15.3	-8.7
ΔQFM	0	-1	+2
pH	4.83	4.91	4.50
a_{H_2O}	0.98	0.98	0.98

(c)	950 °C, 4.5 GPa
ELEMENT	Peridotitic diamond-forming
Na	2.5
K	4.7
Ca	$6.1*10^{-1}$
Mg	$2.3*10^{-1}$
Al	$9.9*10^{-2}$
Si	1.3
Fe	$2.7*10^{-1}$
C	$7.4*10^{2}$
Cr	$6.8*10^{-2}$
log$f$O2 (Pa)	-7.6
ΔQFM	-4
pH	4.64
a_{H_2O}	0.76

(d)	350 °C, Psat (0.017 GPa)
ELEMENT	**Mid-ocean ridge**
Na	$NaCl^0$(55), Na^+(45)
K	K^+(74), KCl^0(26)
Ca	$CaCl_2^0$(60), $CaCl^+$(24), Ca^{2+}(16)
Mg	$MgCl^+$(92), Mg^{2+}(8)
Al	$AlCl_4^-$(79), $AlCl_3^0$(18), $AlOH_4^-$(3)
Si	$SiO_2(aq)$(100)
Fe	$FeCl_2^0$(98), $FeCl^+$(2)
Zn	$ZnCl_4^{2-}$(87), $ZnCl^+$(7), $ZnCl_2^0$(6)
Pb	$PbCl_2^0$(46), $PbCl_3^-$(40), $PbCl_4^{2-}$(11), $PbCl^+$(3)
S	$H_2S(aq)$(100)
C	$CO_2(aq)$(100)
Cr	$CrCl(OH)^0$(100)
log$f$O$_2$	-25.2 Pa
ΔQFM	+1.8
pH	4.79
a_{H_2O}	0.99

(e)	650 °C, 1.0 GPa	570 °C, 2.0 GPa	630°C, 2.0 GPa
ELEMENT	**Pelitic Schist**	**Eclogitic mafic**	**Antigorite ultramafic**
Na	Na^+(85), $NaCl^0$(15)	Na^+(85), $NaHCO_3^0$(11), $NaCl^0$(4)	Na^+(85), $NaHCO_3^0$(8), $NaCl^0$(6)
K	K^+(89), KCl^0(11)	K^+(96), KCl^0(3), KOH^0(1)	K^+(95), KCl^0(5)
Ca	$Ca(H_3SiO_4)^+$(87), $CaCl^+$(11), $Ca(HCO_3)^+$(1)	$Ca(H_3SiO_4)^+$(67), $Ca(HCO_3)^+$(21), $Ca(HCOO)^+$(6), $CaCl^+$(5), Ca^{2+}(1)	$Ca(HCO_3)^+$(56), Ca$(H_3SiO_4)^+$(23), $CaCl^+$(18), Ca^{2+}(2)
Mg	$Mg(OH)_2^0$(96), $Mg(SiO_2)HCO_3^+$(4),	$Mg(SiO_2)HCO_3^+$(61), $Mg(OH)_2^0$(39)	$Mg(SiO_2)HCO_3^+$(52), $Mg(OH)_2^0$(48)
Al	$Al(OH)_3OSi(OH)_3^-$(84), AlO_2^-(9), $HAlO_2(aq)$(7)	$Al(OH)_3OSi(OH)_3^-$ (94), AlO_2^-(5), $HAlO_2(aq)$(1)	$Al(OH)_3OSi(OH)_3^-$ (66), AlO_2^-(19), $HAlO_2(aq)$(15)
Si	$SiO_2(aq)$(50), $Si_2O_4(aq)$(35), $Fe(H_3SiO_4)^+$(11), Ca$(H_3SiO_4)^+$(3), $Al(OH)_3OSi(OH)_3^-$ (1)	$SiO_2(aq)$(50), $Si_2O_4(aq)$(27), $Fe(H_3SiO_4)^+$(10), $Al(OH)_3OSi(OH)_3^-$(5), $Mg(SiO_2)HCO_3^+$(3), $H_3SiO_4^-$(2), Ca$(H_3SiO_4)^+$(2)	$Mg(SiO_2)HCO_3^+$(76), $SiO_2(aq)$(15), $Fe(H_3SiO_4)^+$(7), $Si_2O_4(aq)$(2)
Fe	$Fe(H_3SiO_4)^+$(99), $FeCl_2^0$(1)	$Fe(H_3SiO_4)^+$(73), $Fe(HCOO)^+$(27)	$Fe(H_3SiO_4)^+$(92), $FeCl_2^0$(7), $Fe(HCOO)^+$(1)
C	$H_2CO_3(aq)$(92), $CO_2(aq)$(8)	$CH_4(aq)$(72), $CO_2(aq)$(18), $NaHCO_3^0$(4), $Fe(HCOO)^+$(2), $Mg(SiO_2)HCO_3^+$(2), $HCOO^-$(1), HCO_3^-(1)	$CO_2(aq)$(64), $Mg(SiO_2)HCO_3^+$(34), $NaHCO_3^0$(1),
Cr	$CrCl(OH)^0$(100)	$CrCl(OH)^0$(88), $Cr(OH)_4^-$ (7), $Cr(OH)_3^0$(5)	$CrCl(OH)^0$(87), $Cr(OH)_4^-$ (7), $Cr(OH)_3^0$(6)
log$f$O$_2$	-12.3 Pa	-15.3 Pa	-8.7 Pa
ΔQFM	0	-1	+2
pH	4.83	4.91	4.50
a_{H_2O}	0.98	0.98	0.98

(f)	950 °C, 4.5 GPa
ELEMENT	**Peridotitic diamond-forming**
Na	Na^+(75), $NaCl^0$(17), $NaOH^0$(5), $NaHCO_3^0$(3)
K	K^+(56), KCl^0(41), KOH^0(4)
Ca	$Ca(HSiO)_3^+$(70), $CaCl^+$(26), $CaCl_2^0$(3)
Mg	$Mg(SiO_2)HCO_3^+$(98), $MgCl^+$(2)
Al	$Al(OH)_3OSi(OH)_3^-$(84), $HAlO_2(aq)$(8), AlO_2^-(8)
	$Ca(HSiO)_3^+$(34), $SiO_2(aq)$(31), $Mg(SiO_2)HCO_3^+$(18), $AlO_2(SiO_2)^-$(7), $HSiO_3^-$(6),
Si	$Fe(HSiO_3)^+$(3), $Si_2O_4(aq)$(3)
Fe	$FeCl_2^0$(82), $Fe(HSiO_3)^+$(12), $Fe(HCO_3)^+$(6)
C	$CH_4(aq)$(58), ethane(aq)(27), propane(aq)(12), ethanol(aq)(4)
Cr	$CrCl(OH)^0$(100)
logfO_2	-7.6 Pa
ΔQFM	-4
pH	4.64
a_{H_2O}	0.76

Supplementary Figures

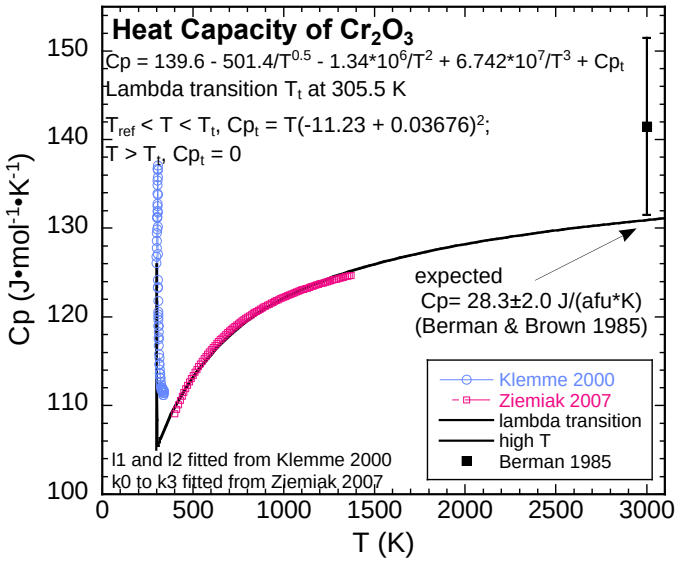

Figure S-1 Fitting of heat capacity for Cr_2O_3 at 10^5 Pa, from 273.15 K to 3000 K, based on experimental data from Klemme *et al*. (2000) and Ziemiak *et al*. (2007).

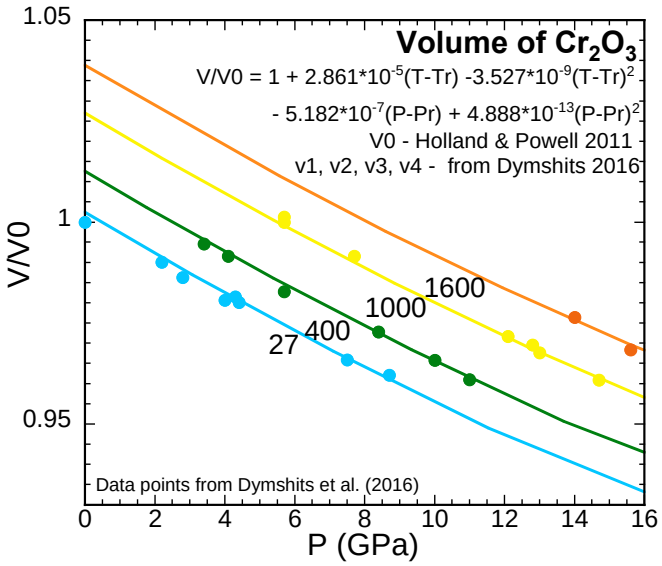

Figure S-2 Fitting of volume for Cr_2O_3 at pressures from 10^5 Pa to 15 GPa, and temperatures from 27 °C to 1600 °C, based on experimental data from Dymshits *et al.* (2016).

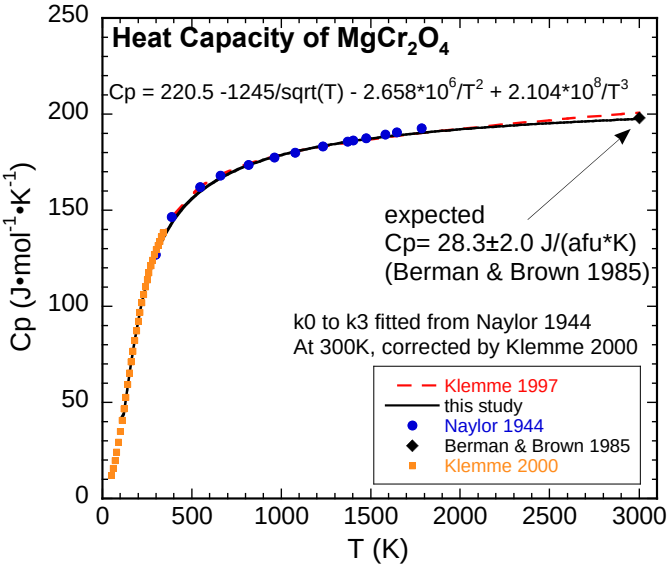

Figure S-3 Fitting of heat capacity for $MgCr_2O_4$ at 10^5 Pa from 0 K to 3000 K, based on experimental data from Klemme and O'Neill (1997), Klemme *et al*. (2000), and Naylor (1944).

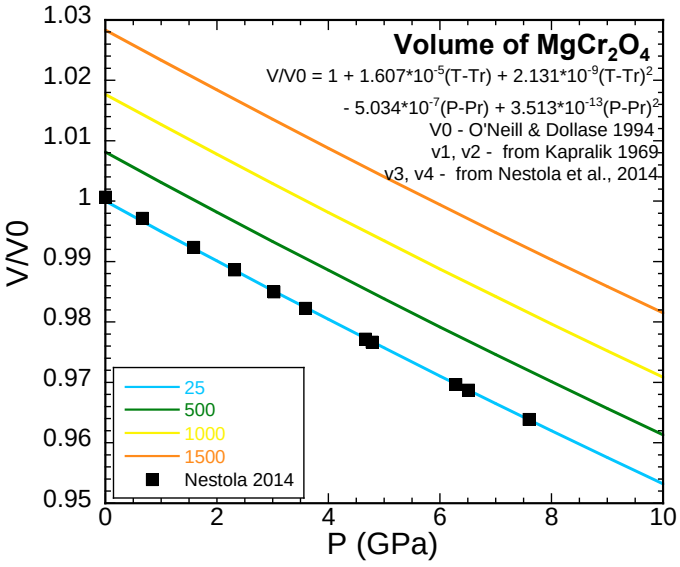

Figure S-4 Fitting of volume for $MgCr_2O_4$ at pressures from 10^5 Pa to 10 GPa, and temperatures from 25 °C to 1500 °C, based on experimental data from Kaprálik (1969) and Nestola *et al*. (2014).

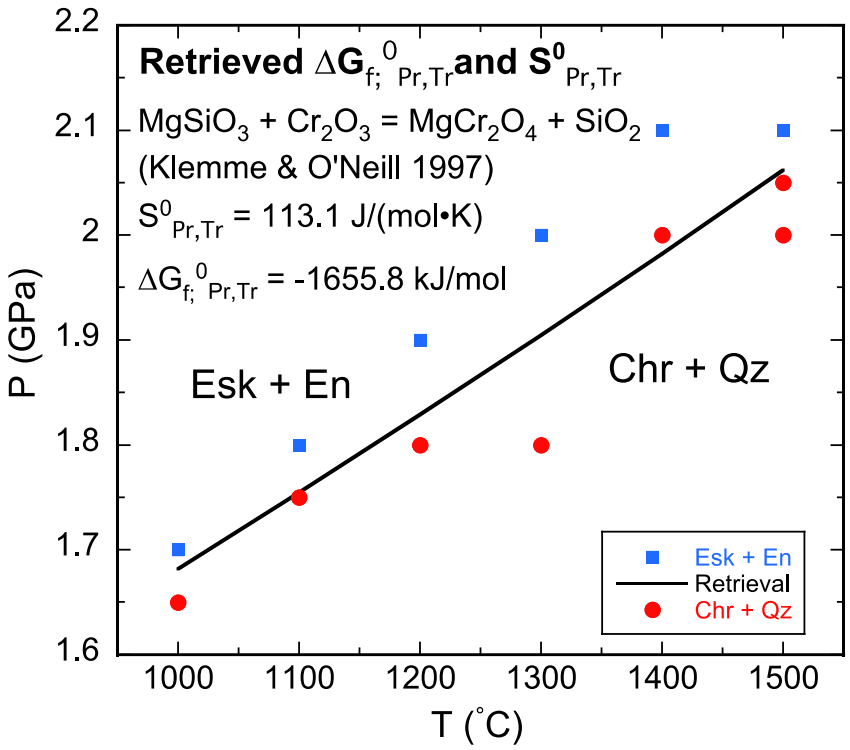

Figure S-5 Retrieval of Gibbs free energy of formation and entropy at 25 °C, 10^5 Pa for $MgCr_2O_4$, based on experimental data from Klemme and O'Neill (1997).

Supplementary Information References

Accornero, M., Marini, L., Lelli, M. (2010) Prediction of the thermodynamic properties of metal-chromate aqueous complexes to high temperatures and pressures and implications for the speciation of hexavalent chromium in some natural waters. *Applied Geochemistry* 25, 242–260.

Asano, T., Le Noble, W.J. (1976) Activation and Reaction Volumes in Solution. *Chemical Reviews* 78, 407–489.

Baes Jr, C.F., Mesmer, R.E. (1981) Thermodynamics of cation hydrolysis. *Am. J. Sci.;(United States)* 281.

Berman, R.G. (1988) Internally-Consistent Thermodynamic Data for Minerals in the System Na2O-K2O-CaO-MgO-FeO-Fe2O3-Al2O3-SiO2-TiO2-H2O-CO2. *Journal of Petrology* 29, 445–522.

Berman, R.G., Brown, T.H. (1985) Heat capacity of minerals in the system Na2O-K2O-CaO-MgO-FeO-Fe2O3-Al2O3-SiO2-TiO2-H2O-CO2: representation, estimation, and high temperature extrapolation. *Contributions to Mineralogy and Petrology* 89, 168–183.

Debret, B., Sverjensky, D.A. (2017) Highly oxidising fluids generated during serpentinite breakdown in subduction zones. *Scientific Reports* 7.

Dellien, I., Hall, F.M., Hepler, L.G (1976) Chromium, molybdenum, and tungsten: thermodynamic properties, chemical equilibria, and standard potentials. *Chemical Reviews* 76, 283–310.

Dellien, I., Hepler, L.G. (1976) Enthalpies of formation of Cr 3+ (aq) and the inner sphere complexes CrF 2+ (aq), CrCl 2+ (aq), CrBr 2+ (aq), and CrSO 4+ (aq). *Canadian Journal of Chemistry* 54, 1383–1387.

Dymshits, A., Iagher, L., Etgar, L. (2016) Parameters influencing the growth of ZnO nanowires as efficient low temperature flexible perovskite-based solar cells. *Materials* 9, 60.

Hao, J. (2016) Geochemical signatures of weathering and surface water chemistry in the late Archean. PhD thesis, Johns Hopkins University, 248 pp.

Huang, F. (2017) Evolution of aqueous fluids, hydrocarbons, and diamond formation in the upper mantle. PhD thesis, Johns Hopkins University, 207 pp.

Helgeson, H.C., Kirkham, D.H., Flowers, G.C. (1981) Theoretical prediction of the thermodynamic behavior of aqueous electrolytes at high pressures and temperatures: IV. Calculation of activity coefficients, osmotic coefficients, and apparent molal and standard and relative partial molal properties to 600oC. *American Journal of Science* 281, 1249–1516.

Holland, T.J.B., Powell, R. (2011) An improved and extended internally consistent thermodynamic dataset for phases of petrological interest, involving a new equation of state for solids. *Journal of Metamorphic Geology* 29, 333–383.

Johnson, D.A., Nelson, P.G. (2012) Improvements in estimated entropies and related thermodynamic data for aqueous metal ions. *Inorganic Chemistry* 51, 6116–6128.

Johnson, J.W., Oelkers, E.H., Helgeson, H.C. (1992) SUPCRT92: A software package for calculating the standard molal thermodynamic properties of minerals, gases, aqueous species, and reactions from 1 to 5000 bar and 0 to 1000°C. *Computers and Geosciences* 18, 899–947.

Kaprálik, I. (1969) Thermal Expansion of Spinels MgCr2O4, MgAl2O4 and MgFe2O4. *Chemical Papers* 23, 665–670.

Klein-BenDavid Ofra, O., Pettke, T., Kessel, R. (2011) Chromium mobility in hydrous fluids at upper mantle conditions. *Lithos* 125, 122–130.

Klemme, S., O'Neill, H.S.C. (1997) The reaction MgCr2O4+ SiO2= Cr2O3+ MgSiO3and the free energy of formation of magnesiochromite (MgCr2O4). *Contributions to Mineralogy and Petrology* 130, 59–65.

Klemme, S., O'Neill, H.S.C., Schnelle, W., Gmelin, E. (2000) The heat capacity of MgCr2O4, FeCr2O4, and Cr2O3at low temperatures and derived thermodynamic properties. *American Mineralogist* 85, 1686–1693.

Meng, Y., Bard, A.J. (2015) Measurement of Temperature-Dependent Stability Constants of Cu(I) and Cu(II) Chloride Complexes by Voltammetry at a Pt Ultramicroelectrode. *Analytical Chemistry* 87, 3498–3504.

Naylor, B.F. (1944) High-Temperature Heat Contents Of Ferrous and Magnesium Chromites. *Industrial and Engineering Chemistry* 36, 933–934.

Nestola, F., Periotto, B., Andreozzi, G.B., Bruschini, E., Bosi, F. (2014) Pressure-volume equation of state for chromite and magnesiochromite: A single-crystal X-ray diffraction investigation. *American Mineralogist* 99, 1248–1253.

O'Neill, H.S.C., Dollase, W.A. (1994) Crystal Structures and Cation Distributions in Simple Spinels from Powder XRD Structural Refinements : and the Temperature Dependence of the Cation Distribution in ZnAl2O4. *Physics and Chemistry of Minerals* 20, 541–555.

Postmus, C., King, E.L. (2005) The Equilibria in Acidic Solutions of Chromium(III) Ion and Thiocyanate Ion. *The Journal of Physical Chemistry* 59, 1208–1216.

Shock, E.L., Sassani, D.C., Willis, M., Sverjensky, D.A. (1997) Inorganic species in geologic fluids: Correlations among standard molal thermodynamic properties of aqueous ions and hydroxide complexes. *Geochimica et Cosmochimica Acta* 61, 907–950.

Slobodov, A.A., Kritskii, A. V., Zarembo, V.I., V., P.L. (1993) THERMODYNAMIC ANALYSIS OF THE CHEMICAL-REACTIONS OF CHROMIUM WITH AQUEOUS-SOLUTIONS. *Russian Journal of Applied Chemistry* 66, 39–48.

Sverjensky, D.A., Hemley, J.J., D'angelo, W.M. (1991) Thermodynamic assessment of hydrothermal alkali feldspar-mica-aluminosilicate equilibria. *Geochimica et Cosmochimica Acta* 55, 989–1004.

Sverjensky, D.A., Shock, E.L., Helgeson, H.C. (1997) Prediction of the thermodynamic properties of aqueous metal complexes to 1000°C and 5 kb. *Geochimica et Cosmochimica Acta* 61, 1359–1412.

Sverjensky, D.A., Harrison, B., Azzolini, D. (2014). Water in the deep Earth: the dielectric constant and the solubilities of quartz and corundum to 60 kb and 1200 C. *Geochimica et Cosmochimica Acta*, *129*, 125-145.

Viete, D.R., Hacker, B.R., Allen, M.B., Seward, G.G., Tobin, M.J., Kelley, C.S., Cinque, G., Duckworth, A.R. (2018) Metamorphic records of multiple seismic cycles during subduction. *Science Advance* 4, eaaq0234.

Von Damm, K.L. (1990) Seafloor hydrothermal activity: black smoker chemistry and chimneys. *Annual Review of Earth and Planetary Sciences* 18, 173-204.

Watenphul, A., Schmidt, C., Jahn, S. (2014) Cr(III) solubility in aqueous fluids at high pressures and temperatures. *Geochimica et Cosmochimica Acta* 126, 212–227.

Ziemniak, S.E., Anovitz, L.M., Castelli, R.A., Porter, W.D. (2007) Thermodynamics of Cr2O3, FeCr2O4, ZnCr2O4, and CoCr2O4. *Journal of Chemical Thermodynamics* 39, 1474–1492.

Ziemniak, S.E., Jones, M.E., Combs, K.E.S. (1998) Solubility and phase behavior of Cr(III) oxides in alkaline media at elevated temperatures. *Journal of Solution Chemistry* 27, 33–66.